NANO LETTERS
Cite This: Nano Lett. 2017, 17, 8005−8011
Letter
pubs.acs.org/NanoLett

Doping Lanthanide into Perovskite Nanocrystals: Highly Improved and Expanded Optical Properties

Gencai Pan,[†] Xue Bai,*[,†] Dongwen Yang,[‡] Xu Chen,[†] Pengtao Jing,[§] Songnan Qu,[§] Lijun Zhang,[‡] Donglei Zhou,[†] Jinyang Zhu,[†] Wen Xu,[†] Biao Dong,[†] and Hongwei Song*[,†]

[†]State Key Laboratory on Integrated Optoelectronics, College of Electronic Science and Engineering and [‡]Key Laboratory of Automobile Materials of MOE, State Key Laboratory of Superhard Materials, and College of Materials Science and Engineering, Jilin University, Changchun 130012, China

[§]State Key Laboratory of Luminescence and Applications, Changchun Institute of Optics Fine Mechanics and Physics Chinese Academy of Sciences, 3888 Eastern South Lake Road, Changchun 130033, China

S *Supporting Information*

ABSTRACT: Cesium lead halide ($CsPbX_3$) perovskite nanocrystals (NCs) have demonstrated extremely excellent optical properties and great application potentials in various optoelectronic devices. However, because of the anion exchange, it is difficult to achieve white-light and multicolor emission for practical applications. Herein, we present the successful doping of various lanthanide ions (Ce^{3+}, Sm^{3+}, Eu^{3+}, Tb^{3+}, Dy^{3+}, Er^{3+}, and Yb^{3+}) into the lattices of $CsPbCl_3$ perovskite NCs through a modified hot-injection method. For the lanthanide ions doped perovskite NCs, high photoluminescence quantum yield (QY) and stable and widely tunable multicolor emissions spanning from visible to near-infrared (NIR) regions are successfully obtained. This work indicates that the doped perovskite NCs will inherit most of the unique optical properties of lanthanide ions and deliver them to the perovskite NC host, thus endowing the family of perovskite materials with excellent optical, electric, or magnetic properties.

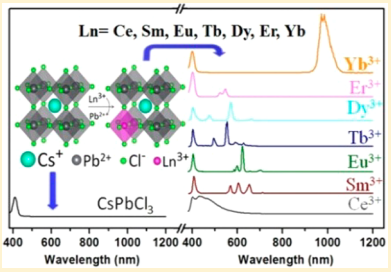

KEYWORDS: *Perovskite nanocrystal, lanthanide, multicolor emissions, near-infrared emissions*

Recently, the metal-halide perovskite nanostructures, in particular the solution-processable cesium lead halide perovskite nanocrystals (NCs), have sprung to the forefront of optoelectronic devices due to their large absorption across, high photoluminescence quantum yield (QY), and especially the narrow band and tunable luminescence over the entire visible spectral region.[1−6] The perovskite NCs' optical property can be easily tailored by quantum-size effect or the individual halide anion exchange due to their nature of high ionic conductivity.[1,7−9] It endows perovskite NCs with the specialty to easily tune their photoluminescence under mild synthesis conditions while both NC morphology and high photoluminescence QY are retained. However, the instability and the lack of coexisted multicolor emissions resulted from the ionic nature of perovskite materials are still the obstacles for their practical applications.[10]

Doping impurity ions has been considered as a promising avenue to control over the electronic, magnetic, and optical performances of NCs.[11,12] To date, several successful substitutions of Pb^{2+} with transition metal ions have been reported for the fully inorganic or hybrid perovskite NCs.[13−17] Nevertheless, the emissions for transition metal ions are broad bands and only confined to several specific wavelength regions owing to their limited energy structures. The lanthanide ions would be the most appropriate candidates because they exhibit rich and unique spectroscopic properties whose emissions are usually sharp lines in the UV to intermediate infrared range.[18−20] Those features can be used for tuning the photoluminescence of perovskite NCs to the desired spectral position. Moreover, moving along the lanthanide series from Ce to Lu, a gradual change in the decrease of ionic radius and the variations of electronic, magnetic, and chemical characterizations[21,22] provide us the opportunities to unveil the underlying mechanism of the doping effect and consequently establish a general principle to conduct the further doping study on perovskite NCs.

To validate these scientific curiosities, we developed a modified hot-injection synthesis method, from which an effective doping of a series of lanthanide ions into $CsPbCl_3$ perovskite NCs was achieved.[14,15] The introduction of lanthanide ions not only results in bright and abundant emissions arising from the energy levels of lanthanide ions, but also considerably enhances the overall photoluminescence QYs of $CsPbCl_3$ NCs. Therefore, the efficient, stable, and widely tunable emissions spanning from visible to near-infrared (NIR) regions are achieved. By the lanthanide ions doping, the properties of perovskite materials are expanded and may be endowed new excellent electric or magnetic properties, which will induce novel optoelectronic applications.

Received: October 26, 2017
Revised: November 21, 2017
Published: November 28, 2017

ACS Publications © 2017 American Chemical Society

DOI: 10.1021/acs.nanolett.7b04575
Nano Lett. 2017, 17, 8005−8011

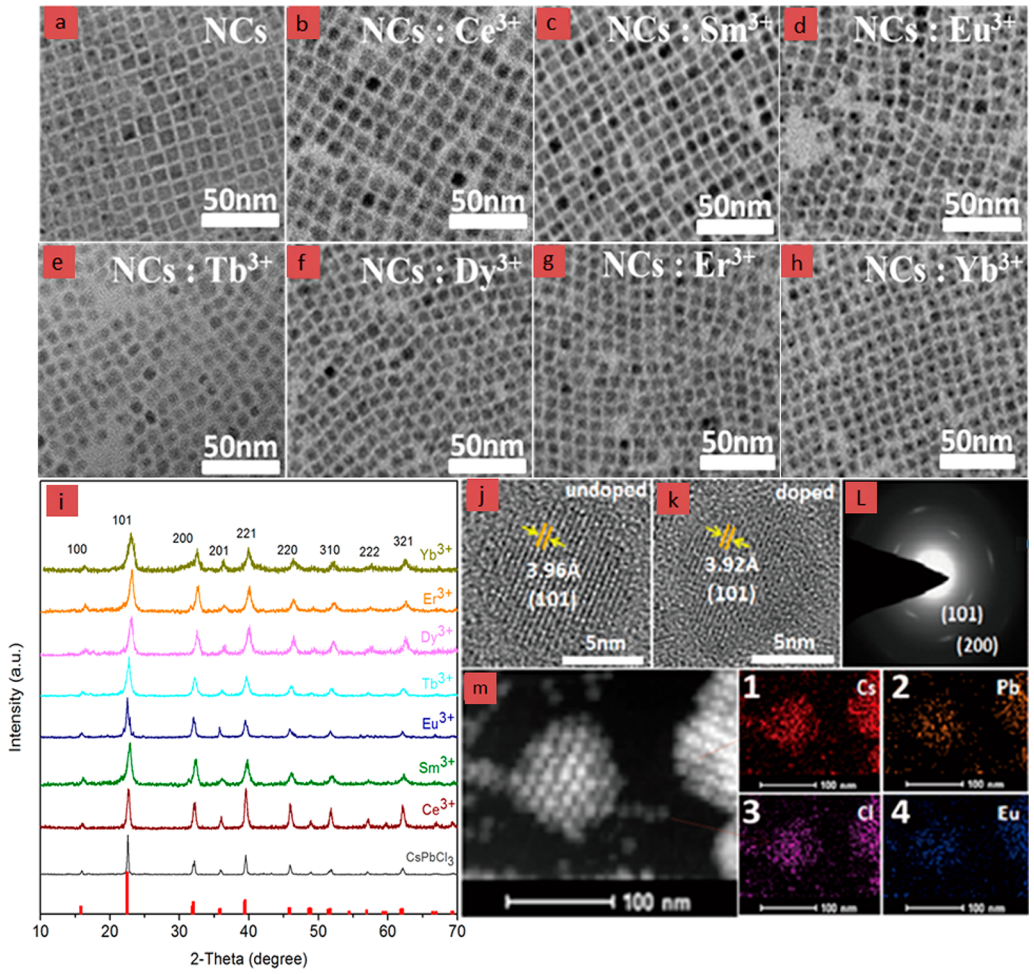

Figure 1. Morphology and structural characterization for the $CsPbCl_3$ NCs doped with different lanthanide ions. (a–h) TEM images, (i) XRD patterns of the $CsPbCl_3$ NCs doped with different lanthanide ions. (j, k) HRTEM images of undoped and Eu^{3+} ions doped $CsPbCl_3$ NCs. (l) SAED pattern of Eu^{3+} ions doped $CsPbCl_3$ NCs. (m) EDX mapping images of Eu^{3+} ions doped $CsPbCl_3$ NCs (hot injection temperature is at 240 °C).

Results and Discussion. All samples were first examined by transmission electron microscope (TEM) technique, and the TEM images imply the large quantity and good uniformity of the as-prepared NCs (Figure 1a–h and Figure S1). With the addition of lanthanide ions, although the NCs preserve the similar cubic shape, the average size of NCs decreases regularly as the atomic number of lanthanide ions increases. X-ray diffraction (XRD) patterns of the as-prepared samples indicate that the perovskite structures are formed in both doped and undoped NCs (Figure 1i), in which a series of diffraction peaks are displayed similarly in the distinct samples, and can be indexed to the planes of tetragonal space group *P4mm* of perovskite structure (JCPDS No. PDF#18–0366). The crystalline lattice constants for the (101) diffraction planes are calculated (Table S1). The lattice constants decrease from 3.94 to 3.87 Å with the increase of atomic number of lanthanide ions from Ce^{3+} to Yb^{3+} ions.

Typical high resolution transmission electron microscopy (HR-TEM) images are shown in Figure 1j and k. The lattice constants of undoped and 7.8 mol % Eu^{3+} ions doped $CsPbCl_3$ NCs are determined to be 3.96 and 3.92 Å, respectively, which are consistent with the XRD calculation results (Table S1). Meanwhile, the HR-TEM images show that undoped and 7.8 mol % Eu^{3+} ions doped $CsPbCl_3$ NCs possess tetragonal crystal structure with corresponding (101) plane. The selected area electron diffraction (SAED) pattern (Figure 1L) for the Eu^{3+} ions doped NCs also revealed the presence of (101) and (200) planes of tetragonal phase, further confirming the formation of perovskite structure. The energy-dispersive X-ray (EDX) analysis and mapping images have proven that the lanthanide elements have been involved in the $CsPbCl_3$ perovskite NCs (Figure S2 and Figure 1m).

To evaluate the possibility of lanthanide ions doped into $CsPbCl_3$ perovskite NCs, the first-principle defect calculations are carried out by using plane-wave pseudopotential methods within density functional theory (DFT) as implemented in the Vienna Ab-initio Simulation Package (VASP).[23−26] The calculation details are presented in the Supporting Information. The available equilibrium chemical potential region for cubic $CsPbCl_3$ is shown in Figure S3a. The result indicates that the thermodynamically stable region for $CsPbCl_3$ perovskite host is quite narrow and the growth condition should be carefully controlled to obtain high quality perovskite NCs. Three types of defects, that is, lanthanide ions in the interstice (La_i), occupying location of Cs (La_{Cs}), and occupying location of Pb (La_{Pb}), are considered in this work. Their defect formation energy as a function of Fermi level is shown in Figure S3b,c. It is found that the formation energy of La_{Pb} as a function of the Fermi level is always the lowest comparing with those of La_i and La_{Cs} regardless of the Pb poor and Pb rich conditions

DOI: 10.1021/acs.nanolett.7b04575
Nano Lett. 2017, 17, 8005–8011

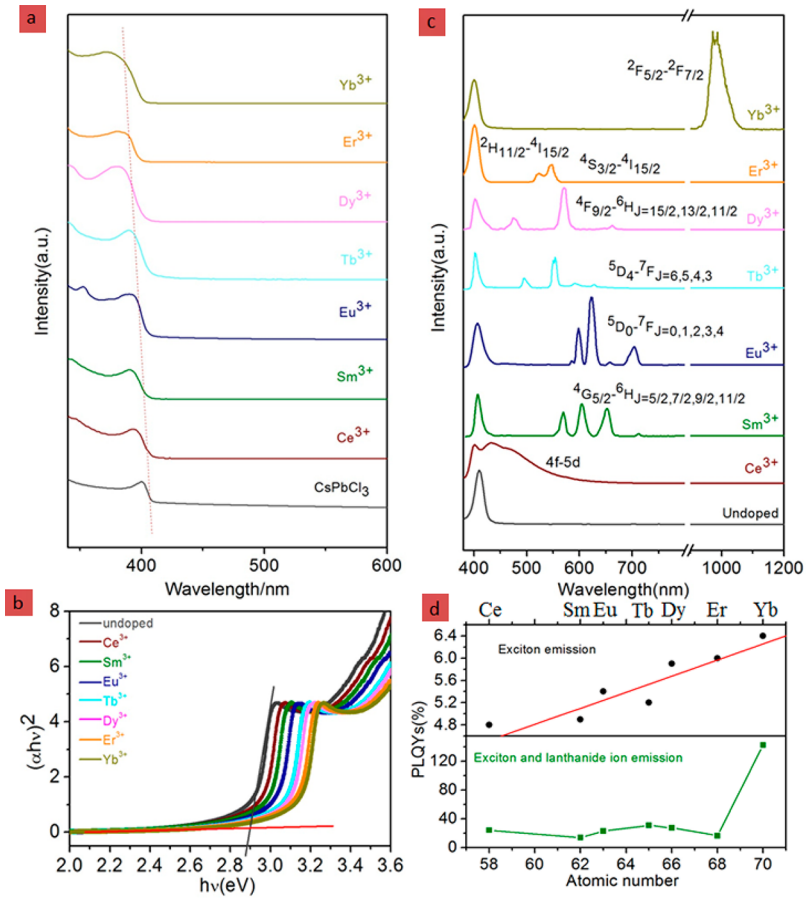

Figure 2. Optical properties of $CsPbCl_3$ NCs doped with different lanthanide ions. (a) Absorption spectra. (b) Tauc plots. (c) Emission spectra. (d) Photoluminescence QYs for excitonic emissions from $CsPbCl_3$ NC host (red line) and for the overall emissions from both NC host and lanthanide ions (green line).

corresponding to A and B points (noted in Figure S3a), which indicates that the lanthanide ions would tend to occupy the Pb^{2+} site.

To further verify the conclusion resulted from the DFT calculation, XPS comparative analyses of undoped and Eu^{3+} ions doped NCs were also performed. The result revealed that the undoped and Eu^{3+} ions doped NCs both comprised Cs, Pb, Cl, C, and O elements (Figure S4a). The high-resolution XPS spectra revealed that the binding energy of Pb^{2+} $4f_{5/2}$ and Pb^{2+} $4f_{7/2}$ decreased obviously as Eu^{3+} ions were introduced, while the binding energies of Cs^+ $3d_{3/2}$ and Cs^+ $3d_{5/2}$ as well as those of Cl^- $2p_{1/2}$ and Cl^- $2p_{3/2}$ exhibited little variations (Figure S4b–d). These results indicate that some Eu^{3+} ions have entered into the lattice of $CsPbCl_3$ perovskite host and most probably replace the Pb^{2+} sites rather than the Cs^+ and Cl^- sites.

Furthermore, the doping concentrations of various lanthanide ions are further identified by the inductively coupled plasma mass spectrometry (ICP-MS) measurements (Table S1). The results show that the overall concentrations of various lanthanide ions distribute in the range from 7.2 to 9.1 mol %. It should be noted that the doping lanthanide ions also have the possibility to exist on the surface of NCs and most probably coordinated by Cl^- ions considering the highly Cl^- ion rich synthetic conditions,[27] which are confirmed through the high-resolution XPS analysis of the doping ion binding energy for the typical Eu^{3+} ions doped sample. In Figure S5, the binding energy of Eu^{3+} $4d_{3/2}$ is related to the Eu^{3+} ions doped into the lattice of NCs,[28] and the binding energy of Eu^{3+} $3d_{3/2}$ can be associated with the $EuCl_3$ anchored on the surface of NCs that is consisting with the reports for the $EuCl_3$ materials in the literatures,[29] readily confirming that the doping ions existed on the surface and also substitute Pb^{2+} lattice site of NC host.

The absorption spectra show that the first excitonic peak of the perovskite host shifts to higher energy with increasing the atomic numbers of doping ions (Figure 2a). The optical band gaps of NC host are quantified from the Tauc plots of $(\alpha h\nu)^2$ versus $h\nu$ (Figure 2b). With increasing the atomic numbers of lanthanide ions, the band gap of the NC host gradually becomes larger due to the lattice contraction of doped NCs.[15] As is well-known, the increase of band gap in semiconductor with the decrease of lattice constant that is also called the band gap engineering of semiconductor was frequently observed in the literature.[15,17] As reported in these works, the decrease of lattice constants induced an enhancement of binding energy between anions and cations, thus leading to the increase of band gap energy.[15,17] However, it should be noted that the particle size decreases from 7.6 to 6.3 nm as the lanthanide ions are involved, which might also lead to the blue shift of band gap in the perovskite NCs based on the quantum confinement effect. To evaluate these two effects, we calculated the variation of band gap depended on the quantum confinement effect from the equation, $\Delta E = \frac{\hbar^2\pi^2}{2m_rR^2} - \frac{1.786e^2}{4\pi\varepsilon_0\varepsilon R}$, where R is the particle radius, m_r is the effective mass of the exciton, and ε is the relative dielectric constant of $CsPbCl_3$ bulk material.[30,31] The

DOI: 10.1021/acs.nanolett.7b04575
Nano Lett. 2017, 17, 8005–8011

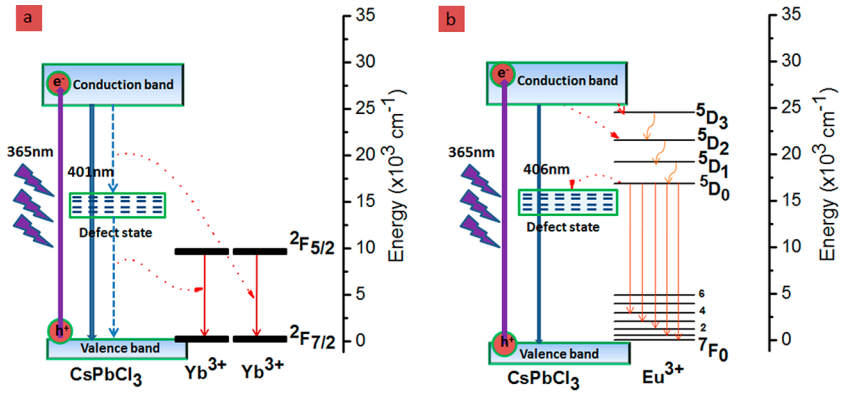

Figure 3. (a) Energy level diagram of Yb^{3+} ions doped $CsPbCl_3$ perovskite NCs and the possible quantum cutting mechanisms. (b) Energy level diagram of Eu^{3+} ions doped $CsPbCl_3$ perovskite NCs and the possible photoluminescence mechanisms.

result shows that the band gap merely shifts about 17 meV as the particle size changes from 7.6 to 6.3 nm, which is much smaller than the practical change of 230 meV (Table S1), thus implying that the quantum confinement effect is not the dominant mechanism for the shift of band gap.

The emission features are revealed by the photoluminescence spectroscopy (Figure 2c). Under the excitation of 365 nm light, the emission spectra for the undoped and lanthanide ions doped $CsPbCl_3$ NCs exhibit a narrow band-edge emission around 410 nm, which is consistent with previous reports,[7] whereas the position shifts continuously to blue with increase of the atomic numbers of doped ions (Figure 2b and Figure S6). Meanwhile, several intense components associated with the intrinsic electronic transitions of lanthanide ions contribute to the emission spectra as noted in the Figure 2c, those are *4f*−*5d* transition for Ce^{3+}, $^4H_{5/2}$-^6H_J (J = 2/5, 2/7, 2/9, 2/11) for Sm^{3+}, $^5D_0$-^7F_J for Eu^{3+}, $^5D_4$-^7F_J (J = 3−6) for Tb^{3+}, $^4G_{5/2}$-^6H_J (J = 15/2, 13/2, 11/2) for Dy^{3+}, $^2H_{11/2}$-$^4I_{15/2}$ /$^4S_{3/2}$-$4I_{15/2}$ for Er^{3+}, and $^2F_{5/2}$-$^2F_{7/2}$ for Yb^{3+} ions. These results indicate that an efficient energy transfer occurs from $CsPbCl_3$ NC host to the energy levels of lanthanide ions because 365 nm light falls in the main absorption band of perovskite NC host (Figure 2c). The excitation spectra selectively monitored at the peak position of lanthanide ions present the broad UV component from 270 to 420 nm, which matches closely with the excitonic absorption of $CsPbCl_3$ NC host (Figure S7), confirming that the emissions of lanthanide ions are sensitized mainly by the $CsPbCl_3$ NC host.

The emission features of the as-prepared lanthanide ions doped NCs are quantified by the absolute emission QY (Figure 2d and Table S1). The doping of lanthanide ions introduces a great enhancement of the overall photoluminescence QY for the doped $CsPbCl_3$ NCs compared with that of the undoped NCs, mainly resulting from the contribution of the intrinsic emission of lanthanide ions. Intriguingly, although the energy transfer occurs from the exciton to lanthanide ions, the photoluminescence QY of excitonic emission of $CsPbCl_3$ NC host increases. Actually, there are two competitive pathways that influence the exciton transitions when introducing lanthanide ions into the $CsPbCl_3$ perovskite NCs. One is the energy transfer from exciton of perovskite host to doping ions, which is generally considered to decrease the photoluminescence QY of exciton.[27] However, researches have reported that some nonradiative recombination pathways (such as Cl vacancy) for exciton transitions of $CsPbCl_3$ perovskite NCs can be removed through the doping of metal ions.[14,27] Therefore, the increase of the photoluminescence QY of exciton mainly results from the modification of the defects in the materials.

Time-resolved spectroscopy provides further details on the mechanism of optical improvement (Figures S8 and S9). The lifetimes associated with the various emission decays of lanthanide ions present a single exponential behavior, which is consistent with the previous reports for the intrinsic transitions of lanthanide ions (Figure S8 and Table S2).[11] The single exponential behavior of lanthanide emission decays in the doped NCs suggests a relatively homogeneous electronic transition environment for the lanthanide ions.[27] It should be noted that although the lanthanide chlorides existed on the surface of NC host, they normally have no detectible photoluminescence under the 365 nm excitation (Figure S10). Under the intrinsic excitation of lanthanide ions, the lanthanide chlorides present extremely low emissions, for example, the $EuCl_3$ in toluene solution demonstrates quite dim $^5D_0$-^7F_J (J = 0,1,2) emissions under 394 nm, which is three-order lower than the present photoluminescence (Figure S10). Therefore, we can conclude that the lanthanide chlorides anchored on the surface of NCs has little influence on the optical properties of lanthanide doped perovskite NCs. Nevertheless, the photoluminescence decay curves of the excitonic transition of the $CsPbCl_3$ NC host can be well fitted by a biexponential function, in which the faster decay component (τ_1) is owing to the quenching of charge carriers and the slower component (τ_2) is associated with the direct radiative recombination of free charge carriers.[32−34] It is clear that the average lifetimes of the doped $CsPbCl_3$ NCs increase slightly with the increase of doping atomic numbers (Figure S9 and Table S3). The prolonged emission decays accompany with the increase of photoluminescence QYs, suggesting that the nonradiative paths are partly eliminated, while the lanthanide ions are introduced into the crystal lattices.

The modification of Cl vacancy of $CsPbCl_3$ perovskite NC host as well as the energy transfer from exciton to lanthanide ions can be further confirmed by the comparative analysis of the exciton relaxation dynamics in the undoped and Eu^{3+} ions doped NCs through the femtosecond transient absorption (fs-TA) spectroscopy. From Figure S11, the recovery of the ground state bleach (GSB) in the undoped $CsPbCl_3$ NCs reveals the presence of two distinct components with time constants of 3.4 ps and 3.5 ns for the faster and slower recovery components, respectively (Table S4). The picosecond-scale recovery component can be attributed to the depletion of the

DOI: 10.1021/acs.nanolett.7b04575
Nano Lett. 2017, 17, 8005−8011

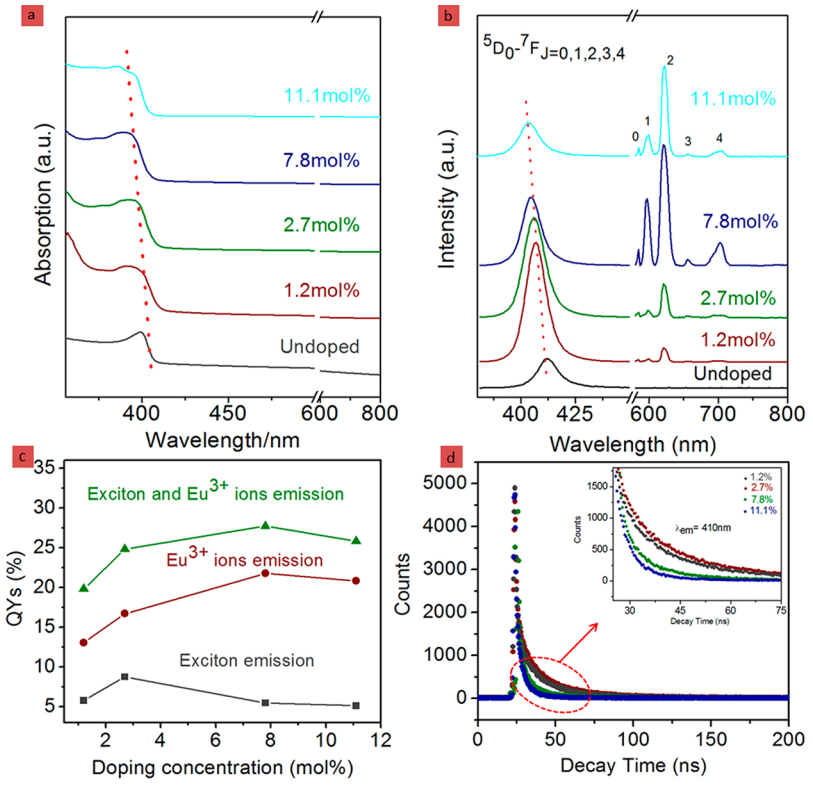

Figure 4. Optical properties of Eu^{3+} ions doped $CsPbCl_3$ NCs with different doping concentrations. (a) Steady-state absorption spectra. (b) Emission spectra under 365 nm excitation. (c) Photoluminescence QYs. (d) Emission decays of excitonic transition monitored at 410 nm (inset is enlarge view of dashed ellipse).

population of $CsPbCl_3$ NC host by the rapid electron trapping to the Cl vacancy, and the slower nanosecond-scale recovery component is related to the combination of radiative and other slower nonradiative recombination of exciton without the fast electron trapping. Those phenomena have been first proposed and investigated thoroughly by Son group.[14,27] By comparing the transient absorption of the Eu^{3+} ions doped NCs with undoped NCs, the picosecond recovery component associated with the rapid electron trapping was prolonged from 3.4 ± 0.7 to 5.2 ± 1.1 ps by the doping of Eu^{3+} ions, indicating that some of the Cl vacancy have been removed. In addition, one new recovery component with time constant of 113 ± 10 ps appears in the Eu^{3+} ions doped NCs. This additional component exactly represents the exciton-doping ions energy transfer being ascribed in literature.[27]

In addition, it is necessary to note that the NIR emission band centered at around 1000 nm associated with the intrinsic transitions of Yb^{3+} ions exhibits a high photoluminescence QY of 143%, which may result from the quantum cutting of excitonic transition of $CsPbCl_3$ NC host.[35−39] A possible photoluminescence mechanism for Yb^{3+} ions doped $CsPbCl_3$ NCs is shown in Figure 3a. Under the excitation of a 365 nm light, the electrons are excited from the valence band into the conduction band of $CsPbCl_3$ NC host and then emit blue photons due to the excitonic recombination. On the other hand, because of the existence of intermediate energy level associated with the defects in the NC host (proved in Figure S12), the electrons in the conduction band can transmit to the defect state and simultaneously transfer excited state energy to a Yb^{3+} ion, and then generate $^2F_{5/2}$-$^2F_{7/2}$ transition. Subsequently, the electrons on defect state further recombine with valence bands and transfer energy to another Yb^{3+} ion. For the other lanthanide ions doped perovskite NCs, the exciton transfer energy to the higher energy level of lanthanide ions and then transmit to the emitting level ($^5D_0$) through the nonradiative relaxation, such as the case of Eu^{3+} ions (Figure 3b), in which some of the exciton energy is depleted by the lattice vibration. Therefore, the photoluminescence QY of Yb^{3+} ions doped NCs is much higher than those of the other lanthanide doped NCs.

We further investigated the doping concentration effect on the optical properties of $CsPbCl_3$ NCs, and the typical experiment was carried out for the Eu^{3+} ions doped samples. The doping concentration is facilely controlled by the injection temperatures during the synthesis and identified by ICP-MS (Table S5). TEM images indicate that the $CsPbCl_3$ NCs with different doping concentrations of Eu^{3+} ions exhibit similar tetragonal morphology (Figure S13a). The crystalline structure is consistent for the NCs doped with different ion concentrations, while the lattice constants of $CsPbCl_3$ NC host decreased with the doping concentration that have been confirmed by the XRD measurement (Figure S13b, Table S6).

The dependence of photoluminescence on the doping concentration is investigated first from the absorption spectra. The first excitonic absorption peak presents a clear blue-shift from 404 to 393 nm with increasing the doping concentration due to the lattice contraction (Figure 4a, Table S7). Under excitation of 365 nm light, the emission spectra for Eu^{3+} ions doped NCs with different doping concentrations reveal the presence of exciton of $CsPbCl_3$ NC host and intrinsic Eu^{3+} ion $^5D_0 \rightarrow {}^7F_J$ (J = 0−4). The similar blue-shift with the absorption features for the excitonic transition also happens in the emission spectra of the excitonic transition (Figure 4b). Interestingly, the relative intensity of intrinsic transitions of

DOI: 10.1021/acs.nanolett.7b04575
Nano Lett. 2017, 17, 8005−8011

Eu^{3+} ions to the excitonic emitting components increases clearly with the doping concentration, which suggests that high doping concentration benefits the energy transfer from NC host to Eu^{3+} ions. The photoluminescence QY as well as emission decays of the NCs doped with different Eu^{3+} ion concentrations are also evaluated (Figure 4c,d). As a function of Eu^{3+} concentration, the photoluminescence QY for the emissions of exciton and Eu^{3+} ions initially increases, and approaches an optimum, and then decreases with the increase of the Eu^{3+} ion doping concentrations. The optimum QY for exciton is achieved at the Eu^{3+} ion doping concentration of 2.7 mol %, while the maximal value for Eu^{3+} ion transition appears at the doping concentration of 7.8 mol %. The overall optimum QY is 27.8%, appearing at the Eu^{3+} concentration of 7.8 mol %. The decay time constant for the exciton transition initially increases (<2.7 mol %) and then decreases with the increase of the Eu^{3+} ion concentration. The initial increase of decay time constant of exciton with Eu^{3+} ion concentration can be attributed to the modification of Cl vacancy through the doping of Eu^{3+} ion, while the subsequent decrease of decay time constant with higher doping concentration is related to the improved energy transfer from exciton to doping ions.

The expanded emissions for various lanthanide ions doped $CsPbCl_3$ NCs are very promising in the light-emitting devices. For instance, because of the unstable red emission for pure $CsPbI_3$-based perovskite NCs,[10] the stability of white LED devices based on perovskite NCs is still a challenge. The stable red emission of Eu^{3+} doped $CsPbCl_3$ NCs is a favorable alternative to fabricate the white LED devices, and the Ce^{3+} ions doped $CsPbCl_3$ NCs possess stable blue and green emission. Therefore, we constructed the Ce^{3+} and Eu^{3+} ions codoped $CsPbCl_3$ NCs and utilized them to produce a white LED by coating them on a commercial ultraviolet LED chip emitting at 365 nm (Figure S14). The LED device exhibits cool white emission (Inset of Figure S14a), and the corresponding emission spectrum is shown in Figure S14a. The color coordinate of the white LED is measured at (0.32, 0.26) (Figure S14b), and the luminous efficiency is 24 lm/W. It is worth to note that the as-fabricated white LED exhibits excellent stability as shown in Figure S15. Moreover, we also found that the colloidal stability of the perovskite NCs has a little increase compared to that of the undoped perovskite NCs by the introduction of lanthanide ions, and the reason for the improved stability will be investigated in details in our further study (Figure S16).

In conclusion, we have successfully developed various lanthanide doped $CsPbCl_3$ perovskite NCs and expanded the family of perovskite materials in terms of optical properties. The introduction of lanthanide ions can considerably improve the photoluminescence QY of $CsPbCl_3$ NCs and easily realize the whole visible light emissions and even NIR emissions, which is particularly significant for light-emitting and other photoelectric devices. The successful doping of lanthanide ions into $CsPbX_3$ perovskite NCs may also endow the material system with excellent electric or magnetic properties, providing a novel platform for optoelectronic applications.

■ ASSOCIATED CONTENT

Supporting Information

The Supporting Information is available free of charge on the ACS Publications website at DOI: 10.1021/acs.nanolett.7b04575.

Detailed synthesis methods and characterization data (PDF)

■ AUTHOR INFORMATION

Corresponding Authors

*E-mail: baix@jlu.edu.cn.

*E-mail: songhw@jlu.edu.cn.

ORCID

Xue Bai: 0000-0003-2309-521X

Songnan Qu: 0000-0003-4159-096X

Lijun Zhang: 0000-0002-6438-5486

Hongwei Song: 0000-0003-3897-5789

Author Contributions

G.C.P., X.B., and H.W.S. designed the experiments, interpreted the data, and cowrote the paper. G.C.P., X.C., P.T.J., S.N.Q., J.Y.Z., D.L.Z., W.X., and B.D. carried out the syntheses, characterizations, optical measurements, and data analyses. D.W.Y. and L.J.Z. performed the DFT calculations. X.B., G.C.P., and H.W.S. discussed and commented on the manuscript.

Notes

The authors declare no competing financial interest.

■ ACKNOWLEDGMENTS

This work was financially supported by the National Natural Science Foundation of China (Grant Nos. 11674127, 11674126, 21403084), Jilin Province Science Fund for Excellent Young Scholars (20170520129JH, 20170101170JC), Major State Basic Research Development Program of China (973 Program) (No. 2014CB643506), and National Key Research and Development Program (2016YFC0207101).

■ REFERENCES

(1) Nedelcu, G.; Protesescu, L.; Yakunin, S.; Bodnarchuk, M. I.; Grotevent, M. J.; Kovalenko, M. V. *Nano Lett.* **2015**, *15*, 5635−5640.

(2) Protesescu, L.; Yakunin, S.; Bodnarchuk, M. I.; Krieg, F.; Caputo, R.; Hendon, C. H.; Yang, R. X.; Walsh, A.; Kovalenko, M. V. *Nano Lett.* **2015**, *15*, 3692−3696.

(3) Song, J.; Li, J.; Li, X.; Xu, L.; Dong, Y.; Zeng, H. *Adv. Mater.* **2015**, *27*, 7162−7167.

(4) Wang, Y.; Li, X.; Song, J.; Xiao, L.; Zeng, H.; Sun, H. *Adv. Mater.* **2015**, *27*, 7101−7108.

(5) Zhang, F.; Zhong, H.; Chen, C.; Wu, X.-g.; Hu, X.; Huang, H.; Han, J.; Zou, B.; Dong, Y. *ACS Nano* **2015**, *9*, 4533−4542.

(6) Sutherland, B. R.; Sargent, E. H. *Nat. Photonics* **2016**, *10*, 295−302.

(7) Palazon, F.; Di Stasio, F.; Akkerman, Q. A.; Krahne, R.; Prato, M.; Manna, L. *Chem. Mater.* **2016**, *28*, 2902−2906.

(8) Sun, S.; Yuan, D.; Xu, Y.; Wang, A.; Deng, Z. *ACS Nano* **2016**, *10*, 3648−3657.

(9) Zhang, D.; Yang, Y.; Bekenstein, Y.; Yu, Y.; Gibson, N. A.; Wong, A. B.; Eaton, S. W.; Kornienko, N.; Kong, Q.; Lai, M.; Alivisatos, A. P.; Leone, S. R.; Yang, P. *J. Am. Chem. Soc.* **2016**, *138*, 7236−7239.

(10) Dastidar, S.; Egger, D. A.; Tan, L. Z.; Cromer, S. B.; Dillon, A. D.; Liu, S.; Kronik, L.; Rappe, A. M.; Fafarman, A. T. *Nano Lett.* **2016**, *16*, 3563−3570.

(11) Wang, F.; Han, Y.; Lim, C. S.; Lu, Y.; Wang, J.; Xu, J.; Chen, H.; Zhang, C.; Hong, M.; Liu, X. *Nature* **2010**, *463*, 1061−1065.

(12) Zhou, B.; Shi, B.; Jin, D.; Liu, X. *Nat. Nanotechnol.* **2015**, *10*, 924−936.

(13) Liu, W.; Lin, Q.; Li, H.; Wu, K.; Robel, I.; Pietryga, J. M.; Klimov, V. I. *J. Am. Chem. Soc.* **2016**, *138*, 14954−14961.

(14) Parobek, D.; Roman, B. J.; Dong, Y.; Jin, H.; Lee, E.; Sheldon, M.; Son, D. H. *Nano Lett.* **2016**, *16*, 7376−7380.

DOI: 10.1021/acs.nanolett.7b04575
Nano Lett. 2017, 17, 8005−8011

(15) Begum, R.; Parida, M. R.; Abdelhady, A. L.; Murali, B.; Alyami, N. M.; Ahmed, G. H.; Hedhili, M. N.; Bakr, O. M.; Mohammed, O. F. *J. Am. Chem. Soc.* **2017**, *139*, 731−737.
(16) Liu, H.; Wu, Z.; Shao, J.; Yao, D.; Gao, H.; Liu, Y.; Yu, W.; Zhang, H.; Yang, B. *ACS Nano* **2017**, *11*, 2239−2247.
(17) van der Stam, W.; Geuchies, J. J.; Altantzis, T.; van den Bos, K. H.; Meeldijk, J. D.; Van Aert, S.; Bals, S.; Vanmaekelbergh, D.; de Mello Donega, C. *J. Am. Chem. Soc.* **2017**, *139*, 4087−4097.
(18) Wang, F.; Deng, R.; Wang, J.; Wang, Q.; Han, Y.; Zhu, H.; Chen, X.; Liu, X. *Nat. Mater.* **2011**, *10*, 968−973.
(19) Zhou, B.; Tao, L.; Chai, Y.; Lau, S. P.; Zhang, Q.; Tsang, Y. H. *Angew. Chem., Int. Ed.* **2016**, *55*, 12356−12360.
(20) Liu, B.; Li, C.; Yang, P.; Hou, Z.; Lin, J. *Adv. Mater.* **2017**, *29*, 2807−2824.
(21) Seitz, M.; Oliver, G. O.; Raymond, K. N. *J. Am. Chem. Soc.* **2007**, *129*, 11153−11160.
(22) Gaunt, A. J.; Reilly, S. D.; Enriquez, A. E.; Scott, B. L.; Ibers, J. A.; Sekar, P.; Ingram, K. I. M.; Kaltsoyannis, N.; Neu, M. P. *Inorg. Chem.* **2008**, *47*, 29−41.
(23) Xu, P.; Chen, S.; Xiang, H.-J.; Gong, X.-G.; Wei, S.-H. *Chem. Mater.* **2014**, *26*, 6068−6072.
(24) Yin, W.-J.; Shi, T.; Yan, Y. *Appl. Phys. Lett.* **2014**, *104*, 063903.
(25) Xiao, Z.; Zhou, Y.; Hosono, H.; Kamiya, T. *Phys. Chem. Chem. Phys.* **2015**, *17*, 18900−18903.
(26) Kang, J.; Wang, L. W. *J. Phys. Chem. Lett.* **2017**, *8*, 489−493.
(27) Rossi, D.; Parobek, D.; Dong, Y. T.; Son, D. H. *J. Phys. Chem. C* **2017**, *121*, 17143−17149.
(28) Schneider, W.-D.; Laubschat, C.; Nowik, I.; Kaindl, G. *Phys. Rev. B: Condens. Matter Mater. Phys.* **1981**, *24*, 5422−5425.
(29) Tan, X. L.; Wang, X. K.; Geckeis, H.; Rabung, T. H. *Environ. Sci. Technol.* **2008**, *42*, 6532−6537.
(30) Brus, L. E. *J. Chem. Phys.* **1983**, *79*, 5566−5571.
(31) Kayanuma, Y.; Momiji, H. *Phys. Rev. B: Condens. Matter Mater. Phys.* **1990**, *41*, 10261−10263.
(32) Liang, P. W.; Liao, C. Y.; Chueh, C. C.; Zuo, F.; Williams, S. T.; Xin, X. K.; Lin, J.; Jen, A. K. *Adv. Mater.* **2014**, *26*, 3748−3754.
(33) Chen, W.; Wu, Y. Z.; Yue, Y. F.; Liu, J.; Zhang, W. J.; Yang, X. D.; Chen, H.; Bi, E. B.; Ashraful, I.; Grätzel, M.; Han, L. Y. *Science* **2015**, *350*, 944−948.
(34) Chen, C.; Li, H.; Jin, J.; Cheng, Y.; Liu, D.; Song, H.; Dai, Q. *Nano Energy* **2017**, *32*, 165−173.
(35) Wegh, R. T.; Donker, H.; Oskam, K. D.; Meijerink, A. *Science* **1999**, *283*, 663−666.
(36) Vergeer, P.; Vlugt, T. J. H.; Kox, M. H. F.; den Hertog, M. I.; van der Eerden, J. P. J. M.; Meijerink, A. *Phys. Rev. B: Condens. Matter Mater. Phys.* **2005**, *71*, 014113.
(37) Ueda, J.; Tanabe, S. *J. Appl. Phys.* **2009**, *106*, 043101.
(38) van der Ende, B. M.; Aarts, L.; Meijerink, A. *Adv. Mater.* **2009**, *21*, 3073−3077.
(39) Ghosh, P.; Mudring, A. V. *Nanoscale* **2016**, *8*, 8160−8169.

DOI: 10.1021/acs.nanolett.7b04575
Nano Lett. 2017, 17, 8005−8011